Unfolding the distribution of periodicity regions and diversity of chaotic attractors in the Chialvo neuron map

Ramírez-Ávila, Gonzalo Marcelo; Muni, Sishu Shankar; Kapitaniak, Tomasz

Published in:
Chaos

DOI:
10.1063/5.0214903

Publication date:
2024

Document Version
Peer reviewed version

Chaos
An Interdisciplinary Journal
of Nonlinear Science

AIP Publishing

Unfolding the distribution of periodicity regions and diversity of chaotic attractors in the Chialvo neuron map

Gonzalo Marcelo Ramírez-Ávila,[1,2,3,a)] Sishu Shankar Muni,[4] and Tomasz Kapitaniak[2]
[1)]*Namur Institute for Complex Systems (naXys), Université de Namur, Rue de Bruxelles 61, B-5000 Namur, Belgium*
[2)]*Division of Dynamics, Lodz University of Technology, Stefanowskiego 1/15, 90-924 Lodz, Poland*
[3)]*Instituto de Investigaciones Fisicas, and Planetario Max Schreier, Universidad Mayor de San Andres, Campus Universitario, C. 27 s/n Cota-Cota, 0000 La Paz, Bolivia*
[4)]*School of Digital Sciences, Digital University Kerala, Technopark Phase IV, Thiruvananthapuram, Kerala 695317, India*

We performed an exhaustive numerical analysis of the two-dimensional Chialvo map by obtaining the parameter planes based on the computation of periodicities and Lyapunov exponents. Our results allowed us to determine the different regions of dynamical behavior, identify regularities in the distribution of periodicities in regions indicating regular behavior, find some pseudofractal structures, identify regions such as the "eyes of chaos" similar to those obtained in parameter planes of continuous systems, and finally, characterize the statistical properties of chaotic attractors leading to possible hyperchaotic behavior.

Keywords: Nonlinear dynamics, chaos, maps, neuron models, Lyapunov exponents, periodicities,self-similarity

Even though there are many tools for analyzing dynamic systems, periodicities and Lyapunov exponents are among the most important due to their capacity to distinguish between periodic and chaotic dynamic behavior. On the other hand, combining these techniques permits obtaining detailed parameter planes that describe the system's fine dynamic features. Thus, when studying the Chialvo map, we identified the well-known shrimp structures indicating the regular behavior of the system; these shrimps follow remarkable sequences, and other structures related to the shrimps are also present following nested arithmetic sequences. The kind of intersection of the shrimps' legs gives rise to a vast grid exhibiting some self-similar properties; nevertheless, the knowledge of the periodicities enables us to discard the fractal scale-free property; consequently, the grids and the elements therein constitute pseudofractals. Other structures, such as the novel "eyes of the chaos," have been found. Another critical concern is the identification of scenarios leading to hyperchaotic behavior that we can estimate from the statistical features of the second Lyapunov exponent and the shape of the concerned attractors.

I. INTRODUCTION

Despite notable advancements in neuroscience in recent years, many unresolved questions about the brain's functionality persist. With millions of neurons serving as the fundamental components of the intricate neural network within the human brain, various types of neurons exist. Since Hodgkin and Huxley conducted their groundbreaking research, numerous models have emerged with the aim of clarifying how neurons function. Neurons exhibit dynamic behavior, firing and bursting, categorizing them as dynamical systems. Examples of continuous neuron systems include the Hindmarsh-Rose[19], Hodgkin-Huxley[20], and FitzHugh-Nagumo models[11], while discrete neuron maps include the Rulkov[35,43], Nekorkin[49], discrete Izhikevich neuron map[22], discrete Hindmarsh-Rose neuron map[28] and Chialvo maps[5,30,34,46,51]. Research has directed significant attention to continuous neuron systems, while discrete mappings have received comparatively less focus. However, in recent years, there has been a notable increase in extensive studies on discrete neuron maps, as referenced in[7,21]. Exploring discrete maps offers numerous advantages, including simplicity, computational efficiency, and applicability in understanding synchronization phenomena. Moreover, they contribute to developing control strategies to modulate neuronal activity, which can help explore therapeutic methods in brain disorders. In summary, including discrete neuron maps in neurodynamics improves our results of neuronal dynamics and their relevance to normal brain function and dysfunction.

One-parameter bifurcation diagrams have turned out to be very useful in finding period-doubling routes to chaos and many other important phenomena. Two-parameter scans are most efficient in detecting various bifurcation scenarios. They are much more powerful than one-parameter bifurcation diagrams as they convey essential information on the dynamics when two parameters simultaneously vary. They have proven useful in detecting various routes of bifurcation of periodic[29], detecting routes to chaos and hyperchaos[10]. Even in higher dimensional systems, the two-parameter scans are very effective, as they have proven to successfully detect many novel bifurcations in them, which are absent in lower dimensional systems.

In these two-parameter scans of nonlinear systems, the prevalence of stability regions indicating regular dynamical behavior is much more common and adopt a variety of shapes other than the usual Arnold tongues, as shrimp-like[13] and

[a)]gonzalo-marcelo.ramirezavila@unamur.be

ring-like[38] shapes, representing the periodicity regions and their boundaries indicate various types of route to chaos. The structure of these regions carries a lot of information about various codimension-one bifurcation curves like the saddle-node bifurcation curve, period-doubling curve, and Neimark-Sacker curve. Moreover, they depict the boundaries of these resonance regions, marking the transition between different dynamical regimes and serve as indicators of various codimension-one bifurcations[53]. Arnold tongues are signatures of stability and predictability of a dynamical system[8]. They are not affected by the dimension of the system and always manifest themselves in two-parameter scans. Boundaries of these structures give an idea of various bifurcation curves as a function of the specified parameters, and they help to identify transitions from periodic to quasiperiodic and chaotic behavior based on color coding according to their largest Lyapunov exponents (LLEs) or their periodicities. They are useful in applications ranging from ecological models[41] to electronic circuits[23] and engineering[3,16,26]. On the other hand, such structures help understand the phenomenon of mode-locking and synchronization in coupled nonlinear oscillators[45], and in particular for the Chialvo map[2,4,52]. The parameter values inside these structures specify where the dynamics of oscillators are mode-locked, leading to synchronization. This aspect is of particular interest in the synchronization of neuronal networks and normal functioning of the brain[6]. In systems characterized by spatial patterns, such as reaction-diffusion systems[25], the concept of stable structures in the parameter space can be extended to study the formation and stability of spatially localized patterns.

Recently, two-dimensional scans were used to understand the distribution of periodicity regions in the Rulkov neuron map[36] and that motivated analysis based on Poincaré maps of this system[54]. Following the same line of a deep analysis based on parameter planes, we have performed in this work a detailed two-parameter study on the two-dimensional discrete Chialvo neuron map, where we show throughout the paper a detailed grid structure that allows us to derive a simple relationship in identifying the periodicity of periodic structures surrounded by four other periodic regions.

Farey rules are helpful in understanding how bifurcations manifest in parameter space, facilitating the identification of critical parameter values where bifurcation points occur[44]. By analyzing the distribution of Farey fractions, researchers can uncover hidden symmetries[12], periodic structures, and topological features within parameter space. In the field of control theory, understanding the distribution of Farey fractions can aid in designing control strategies that stabilize chaotic systems or exploit bifurcations for desired functionality[1].

In 1990, Rössler coined the term hyperchaos to denote chaotic behavior in systems with at least two positive Lyapunov exponents[42]. Since then, hyperchaos has been found in many theoretical dynamical systems as well in many experimental systems like shallow water systems[50], Sommerfeld effect[31], inductorless motor[9]. Various routes and mechanisms to hyperchaos were also studied[48]. We are unaware of the presence of hyperchaos in the two-dimensional Chialvo neuron mapping, although several works refer to this aspect on the Chialvo map[53,56]. Motivated, we approached finding the existence of hyperchaos in the Chialvo map in a heuristic way, analyzing the shape of the chaotic attractor and their simple statistical features concerning the second Lyapunov exponent in several points of a section of the parameter space, where we estimate possible hyperchaotic behavior with all two positive Lyapunov exponents.

Moreover, we also point out that, in line with previous studies on the Chialvo map, see[53], which indicated the presence of self-similarity of a two-parameter scan. In this study, after extensive research, we confirm the self-similarity only in the inner part of the cell-like structures but discard the scale-free fractal property, indicating the pseudofractality of these structures.

The paper is organized as follows. In Sect. II, we present the model and give indications about the Lyapunov exponents and periodicities computation. In Sect. III, we show our results and discuss them, emphasizing the identification of dynamical behavior using LLEs, periodicities, and a combination of both; we also refer to some pseudofractal structures appearing in the parameter planes, and we also point out the chaotic attractor's shapes and the possible existence of hyperchaos. Finally, we outline the conclusions and discuss future directions of the work.

II. MODEL AND METHOD

We focus our analysis on the discrete two-dimensional Chialvo's neuron model given by the map:

$$\begin{aligned} x_{n+1} &= x_n^2 \mathrm{e}^{y_n - x_n} + k, \\ y_{n+1} &= a y_n - b x_n + c\,, \end{aligned} \tag{1}$$

where the variables x and y stand for the activation and recovery of the neuron respectively; whereas the parameters are considered as constants, being a, the time recovery factor, b, the activation dependence factor of the recovery process, c, the offset, and k_0, a constant bias[30].

We iterate Eqs. (1) for 10^6 steps with a transient of $9{\times}10^5$. The importance of choosing such huge values is related to a situation in which the number of iterations is not enough to achieve the final regime of the system, as stated in[54]. With these iterative features, we can compute the Lyapunov exponents, but for the first part of this work, we focus on the LLE, which is computed using the definition[47]:

$$\lambda_1 = \lim_{N\to\infty} \frac{1}{N} \sum_{n=0}^{N-1} \ln \left| \frac{\Delta S_{n+1}}{\Delta S_n} \right| , \tag{2}$$

with

$$(\Delta S_1)^2 = (j_{11}\Delta x_0 + j_{12}\Delta y_0)^2 + (j_{21}\Delta x_0 + j_{22}\Delta y_0)^2 \,,$$

where j_{ik} are the components of the monodromy matrix, which, in our case, is given by

$$J = \begin{pmatrix} x(2-x)\mathrm{e}^{(y-x)} & x^2\mathrm{e}^{(y-x)} \\ -b & a \end{pmatrix} . \tag{3}$$

Consequently, the LLE can be written as:

$$\lambda_1 = \lim_{N\to\infty} \frac{1}{2N} \sum_{n=0}^{N-1} \ln \left[\frac{(j_{11} + j_{12} y'_n)^2 + (j_{21} + j_{22} y'_n)^2}{1 + {y'_n}^2} \right] ,$$

where

$$y'_{n+1} = \frac{j_{21} + j_{22} y'_n}{j_{11} + j_{12} y'_n} .$$

In this manner, it is possible to compute the LLE and to proceed to characterize the details of the parameter planes for unveiling the shape of the stability phases, as shown in Fig. 1. On the other hand, the second LE can be obtained by averaging $\ln|j_{11}j_{22} - j_{12}j_{21}|$ that varies along the orbit. Consequently, the second LE might be written as:

$$\lambda_2 = \langle \ln|j_{11}j_{22} - j_{12}j_{21}| \rangle - \lambda_1 .$$

The other method to come out with the dynamic details of the parameter planes is the computation of periodicities going up to 10^4. In most cases, we considered the total number of iterations to be 10^6 with a transient of 9×10^5 and the distinction between the values that repeat in a cycle with a precision of 10^{-10}. The resolution of most of the parameter planes is 1000×1000 pixels, except those shown in Figs. 1(d), 3 and 5 which have a resolution of 2000×2000 pixels.

III. RESULTS AND DISCUSSION

Using the methods stated in Sect. II allows computing LLEs and periodicities to characterize the dynamic behavior of Chialvo's neuron, devoting special attention to the parameter planes b vs. a.

A. Distinguishing dynamic behavior

In order to characterize the dynamical behavior of Chialvo's neuron model, we describe its inherent dynamic in different sections of the parameter plane by considering the computation of the largest Lyapunov exponents (LLEs). As stated above, some recent works[30,53] have characterized important dynamical aspects of the Chialvo's neuron. Here, we utilize some of these works as the basis for an in-depth analysis of the dynamics of this system. We firstly obtain a parameter plane b vs. a for a vast region, in which it is possible to distinguish fixed point, quasiperiodic, periodic, chaotic and unbounded solutions as shown in Fig. 1, where we note that the region exhibiting periodic behavior has a comb-shape like structure with the teeth oriented to the left or to the right as zoomed in Fig. 1(b) and (c) respectively. In both Figs. 1(b) and (c), we observe in the right part a grid with rhomboids showing a self-similar structure, and also, it is possible to identify the so-called shrimp structures whose "legs" give rise to the rhomboid. On the other hand, inside the rhomboids, a pattern of shrimp distribution is present, an aspect that we discuss in Sect. III C. In Fig. 1(d), we depict a parameter plane k_0 vs a where several dynamic regimes are distinguished. Among them are noted fixed points attained by a fast process or by damped oscillations, quasiperiodic, periodic, and chaotic.

Figure 2 shows some examples of time series (first row) and attractors (second row) obtained in the parameter plane k_0 vs. a of Fig. 1(d). Thus, in Fig. 2(a1), when we consider a point located in the lower left part of the parameter plane ($a = 0.8725$ and $k_0 = 0.03252$), we observe a short transient to attain the fixed point, which is represented in the phase space of Fig. 1(a2); in Fig. 2(b1), the time series shows a damped oscillation to attain the fixed point taken from the upper right part of the parameter plane ($a = 0.8996$ and $k_0 = 0.09892$) that in the phase space is represented by a spiral trajectory as depicted in Fig. 2(b2); on the boundary separating the regions of damped oscillations and quasiperiodicity ($a = 0.8964$ and $k_0 = 0.06198$), the time series shown in Fig. 2(c1) manifests the coexistence of at least two frequencies on the damped oscillations, which in the phase space gives rise to a comb-shape attractor typical of a Neimark-Sacker bifurcation represented in Fig. 2(c2); inside the quasiperiodic region ($a = 0.8959$ and $k_0 = 0.05331$), we observe in the time series of Fig. 2(d1) the oscillatory behavior when there are two or more coexisting frequencies, which result in a torus manifold in the phase space of Fig. 2(d2); finally, Figs. 2(e1)–(e2) ($a = 0.8975$ and $k_0 = 0.03026$) display chaotic time series and the corresponding chaotic attractor respectively.

B. Pseudofractals

Since the seminal work of Mandelbrot[27] to the recently published literature[17], there is a common agreement that fractals exhibit self-similarities and a scale-free feature. In Figs. 1(b) and (c), we stated the self-similarity in the grid structure. This feature is exacerbated when we only consider the difference between regular and chaotic behavior in a part of the grid, as shown in the first column of Fig. 3, where in Fig. 3(a) there is a grid formed with the "legs" of the main periodic structures. In each cell, a primary "shrimp" and sequences of secondary shrimps are present, as shown in Fig. 3(b). The grid exhibits self-similarity, and it is clear that in the absence of the coordinates when focusing on a cell, it is impossible to detect where such a cell is located in the grid; the latter drives to the scale-free property. The properties mentioned above lead us to the main features of a fractal structure.

Nevertheless, when one observes the same Figs., but described in terms of the LLEs as shown in Figs. 3(c)–(d), the self-similarity property seems to be preserved, but the scale-free property vanishes because of the information given by the LLEs. The loss of the scale-free property is still more evident when we represent the same parameter planes in terms of periodicities, as shown in Figs. 3(e)–(f). Consequently, it is possible to refer to the grid and cells appearing in the parameter planes of Fig. 3 as pseudofractals. It is interesting to note that similar structures have been found and described in a continuous system, namely the Chua's circuit in its original form with a piecewise linear function and also with the cubic approximation form[37,39]; in the works mentioned above,

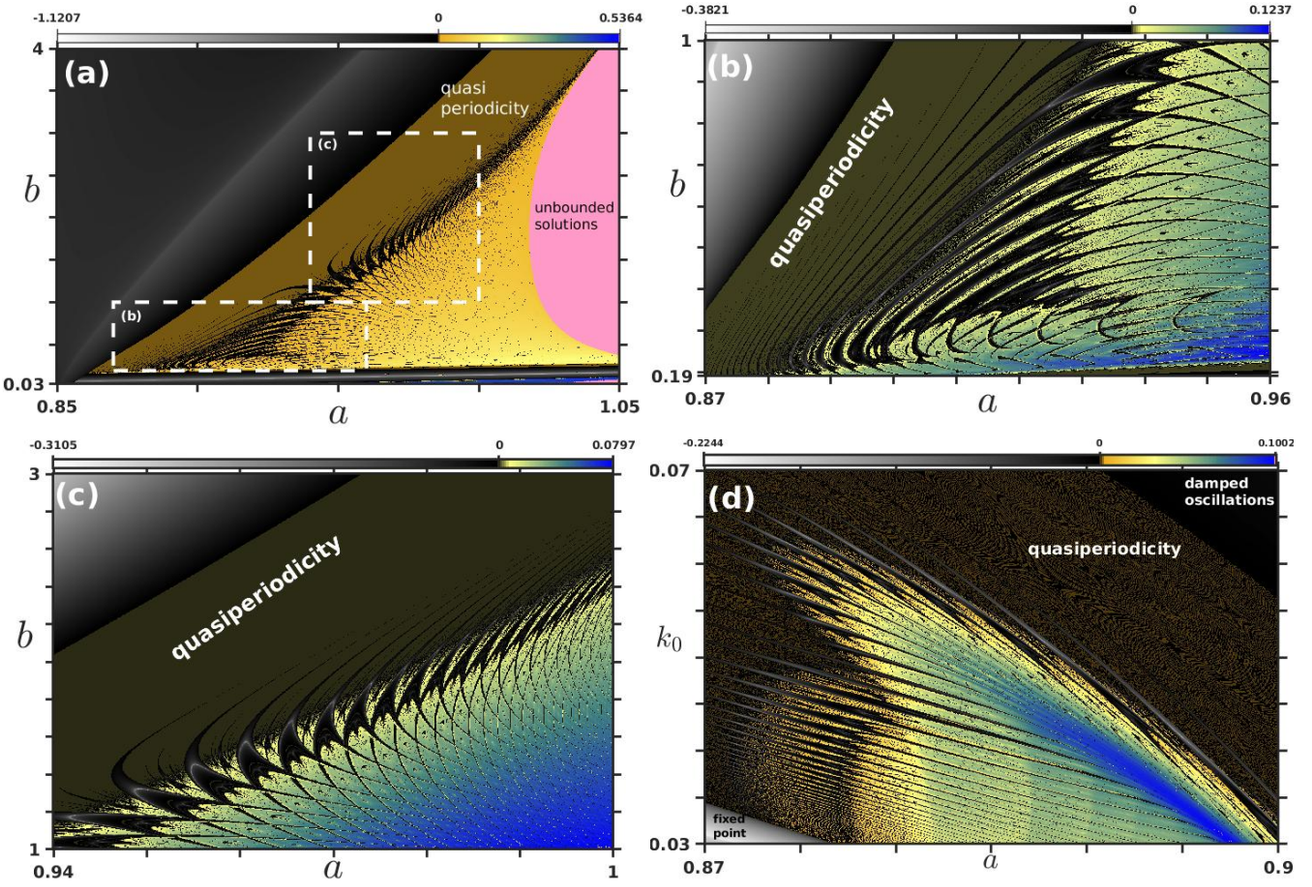

Figure 1. (a) Parameter plane b vs a in terms of the LLEs, keeping constant $c = 0.28$ and $k_0 = 0.04$ with initial conditions $x_0 = 0.1$ and $y_0 = 0.12$. (b) and (c) Zoom of the rectangular regions shown in (a). (d) Parameter plane k_0 vs a in terms of the LLEs, keeping constant $b = 0.18$ and $c = 0.28$ with the same initial conditions as in (a)–(c). The color bar indicates the LLE values.

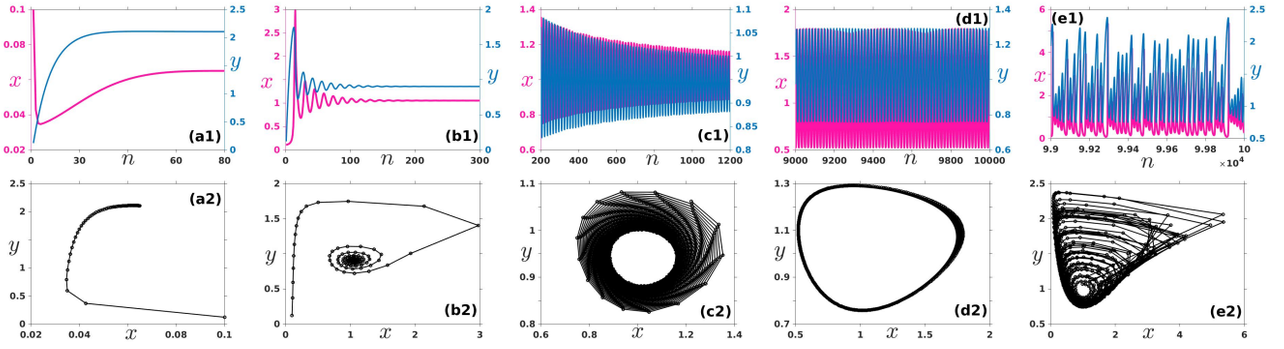

Figure 2. Time series (first row) and attractors (second row) representing the dynamical behavior of different parameter sets of the plane k_0 vs. a of Fig. 1(d) with $b = 0.18$ and $c = 0.28$ and initial conditions $x_0 = 0.1$ and $y_0 = 0.12$. (a) Fixed point with $a = 0.8725$ and $k_0 = 0.03252$. (b) Damped oscillations towards a fixed point with $a = 0.8996$ and $k_0 = 0.09892$. (c) Damped oscillations towards a closed invariant curve with $a = 0.8964$ and $k_0 = 0.06198$. (d) Quasiperiodic regime with $a = 0.8959$ and $k_0 = 0.05331$. (e) Chaotic behavior with $a = 0.8975$ and $k_0 = 0.03026$.

the description of the pseudofractal structures has been made distinguishing the regular from the chaotic behavior as in the first column of Fig. 3 and also using the LLEs as in the second column of Fig. 3, and even the authors computed the fractal dimension considering only the geometrical self-similarities[39]. The information given by the representation in terms of periodicities combined with the LLEs offers exhaustive details on the system's dynamical behavior, and we present such representations in Sect. III C. As a glimpse of the periodicity distribution, Fig. 3(f) indicates the periodicity of the main shrimps inside the cell. It is possible to find recurrent formulas for the main periodicity of any shrimp contained in a cell, as pointed out in Sect. III C and in particular in Fig. 5.

C. Distribution of periodicity regions

In the precedent Sect. III B, we introduced the description of the parameter planes in terms of periodicities. These quantities are computed as indicated in Sect. II. For the analysis, we consider Figs. 1(b)–(c) but expressed in terms of periodicities as shown in Figs. 4(a)–(b), where the different dynamical behaviors (fixed point, quasiperiodic, periodic, and chaotic) and also the shapes of the structures denoting regular oscillatory behavior characterized by specific colors are distinguishable.

We note in Fig. 4(a) that the shrimps' "head" are left-downward oriented and the main periodicity diminishes in the downward direction; we also observe in the bottom part that there is a strong shrimps' deformation, giving rise to some structures observed already in the parameter planes of continuous systems as the so-called "eye of the chaos"[14,15,40,55]. In our case, a zoom of the rectangular region of Fig. 4(a) shown in Fig. 4(c) allows one to observe that there are two "eyes of chaos" resulting from the deformed shrimp with a periodicity of 27 and in an inner period-doubling bifurcation. Interestingly, other "eyes of the chaos" are observed in the secondary structure, whose main periodicity is 59, between the deformed shrimps with main periodicities of 29 and 30, respectively. On the other hand, a magnification of the rectangular region shown in Fig. 4(d) permits one to perceive details of the grid structure formed with the shrimps' legs as depicted in Fig. 4(d). It is important to note that inside each cell on the grid, there is a primary shrimp, as it is labeled in several of these cells. Focusing on the periodicity of the primary shrimp in each cell, we note trends in the main periodicity of the primary shrimps in contiguous cells. Thus, when considering the cell sequence directed to the bottom-right (yellow arrow), we note that the main periodicity of the primary shrimp diminishes by one in this direction, and one also observes that the cell size decreases. The inspection of the cell sequence directed to the right (green arrow) indicates the increase of the main periodicity of the primary shrimp by one, and the cell sizes decrease in this direction; a similar situation occurs when we examine the cell sequence directed to the upper-right part (cyan arrow), where the main periodicity of the primary shrimp increases by two between contiguous cells and as in the precedent case, the cell sizes decrease in this direction. The sequence between two cells that are not nearest neighbors (magenta arrow) remains invariable in the main shrimps' periodicities with decreasing cell sizes when going toward the lower-right part. The abovementioned observations are not surprising because they are concordant with Fig. 1(a), where the sequences of the latter cases will eventually tend to a fixed point or infinity, and the cell sizes become smaller. Finally, Fig 4(f) represents a sketch of an arbitrary region of the grid where we consider a reference cell with the primary shrimp's main periodicity given by p. The main periodicity of the shrimps of the nearest neighbor cell increases by one whether the cell is located at the right or the upper part with respect to the reference cell; on the contrary, this periodicity decreases by one when the nearest neighbor cell is at the left or the lower part. The primary shrimp's periodicity of the next (second) neighbor cells in the direction of the shorter diagonal increases (decreases) by two, whether the cells are located in the right-upper (left-lower) part with respect to the reference cell; on the other hand, when the next neighbor cell is located in any of the longer diagonal direction, the primary shrimp's periodicity remains invariable.

As mentioned before, the colored parts of a cell on the grid represent regions in which the system behaves in a regular way as opposed to the black regions indicating chaotic behavior. Moreover, it was also stated that inside a cell on the grid, there are well-defined inner substructures; for instance, it is noticeable that inside each cell, there is a primary shrimp, and around it, sequences of other shrimps appear. Now, we heed the periodicity distribution exhibited by such shrimps. In order to enhance the visualization, we change the chaotic regions from black to white, and we maintain the colorful representation for the structures indicating periodic behavior as it is shown in Fig. 5, which serves to exemplify how to compute the main periodicity of any of the inner structures of a cell. Firstly, let us consider Fig. 5(a), for which we are supposed to know the main periodicity of the shrimp legs delimiting the cell, which have a "curved parallelogram" shape; we identify the main periodicity of each side by l, t, r, and b, indicating the left, top, right, and bottom sides, respectively. Thus, it is possible to determine the main periodicity of inner shrimp in terms of l, t, r, and b as shown in Fig. 5(a) where we can see that (i) the sides exhibit a period-doubling bifurcation in the direction of concavity. (ii) The primary shrimp has a periodicity of $l+t$ and its head is oriented to the vertex formed by l and t. (iii) Between the left antenna of the primary shrimp and the leg, there is a sequence of secondary shrimps directed to the bottom, whose main periodicity for each of them is given by $l+r+b$, $t+r+b$ and $l+t+b$ respectively. (iv) Similarly, between the right antenna of the primary shrimp and the leg, there is a sequence of secondary shrimps directed to the right, whose main periodicity for each of them is given by $t+r+b$, $l+r+b$ and $l+t+r$, respectively. (v) In the direction of the main shrimp's head, there are two secondary shrimps, one closer to the left side and the other closer to the top side, whose periodicities are given respectively by $t+r+b$ and $l+r+b$. (vi) In the same direction as the primary shrimp's head, there is a tertiary shrimp whose main periodicity is given by $l+t+r+b$. (vii) the precedent relationships

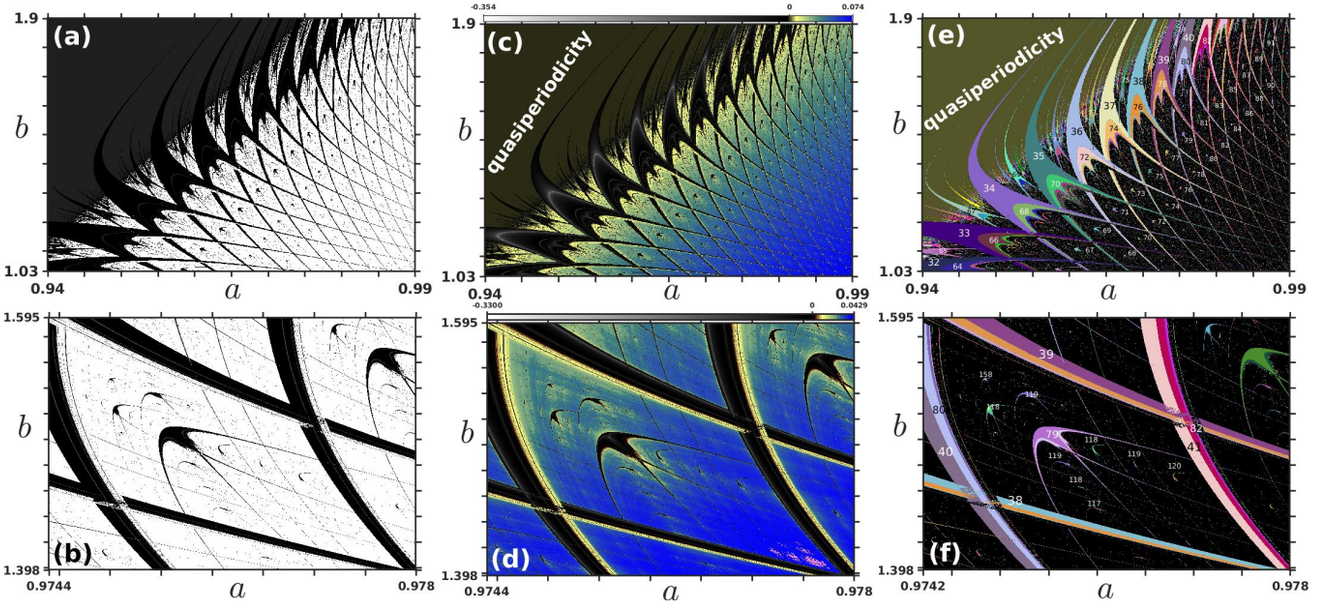

Figure 3. Parameter planes b vs a showing the distinction between regular and chaotic behavior using a binary relation (first column), largest Lyapunov exponents represented by LLE or λ_1 (second column), and periodicities (third column) when $c = 0.28$ and $k_0 = 0.04$, and with initial conditions $x_0 = 0.1$ and $y_0 = 0.12$. For (a), (c), and (e) (first row), we consider the region defined in the intervals: $a \in [0.94, 0.99]$ and $b \in [1.03, 1.9]$. For (b), (d), and (f) (second row), we consider the region defined in the intervals: $a \in [0.9744, 0.978]$ and $b \in [1.398, 1.595]$. Note that regular and chaotic behaviors are characterized respectively by black and white (first column), by a black and white scale with $\lambda_1 \leq 0$, and a color scale with $\lambda_1 > 0$ (second column), and by colors indicating periodicity $\{p : p \in \mathbb{N}^+ \setminus \{1\}\}$ and black (third column).

are valid for any other cell considering the respective periodicity values l', t', r', and b'. Figure 5(b) shows the periodicity values when $l = n$, $t = n-1$, $r = n+1$ and $b = n-2$, where the primary shrimp has a periodicity of $2n-1$, the secondary shrimps are characterized by periodicities from $3n-3$ to $3n$ and the observed tertiary shrimps with $4n-2$ and $4n-3$. With the aim of having more details, we represent in Fig. 5(c) a magnified sight of the primary shrimp of the cell, and in Fig. 5(d), the upper-left part of the cell. We indicate the periodicity of the more visible structures using both notations, i.e., based on the periodicities featuring the sides of the rhomboid (l, t, r, b) and on n. In these zoomed views, secondary, tertiary, and even quaternary shrimps are identified. The latter relationships can be applied and validated using the cell shown in Fig. 3(f), where $n = 40$.

D. Diversity of chaotic attractors

As observed before, chaotic behavior is one of the most predominant in the parameter planes shown before. Nevertheless, in the representation using periodicities, there are no indications of how chaotic the system is because chaos is determined by default when the periodicity cannot be detected after a large number of iterations. Conversely, when computing the Lyapunov exponents, we have a more precise indication of whether the system displays chaotic dynamics or not. A detailed description of Lyapunov exponents is presented in[33]. Alternatively, there are other methods to "quantify" chaos, such as fractal dimensions, correlation dimensions, Kolmogorov-Sinai entropy, and invariant probability measures, among others[18]. With the aim of unveiling the latter question, we choose five different time series (in the interval $[9.998, 10] \times 10^6$) with their respective chaotic attractors (considering the last 10^4 iterations) as depicted in Fig. 6; each case is characterized by its coordinates in the parameter plane and its LLE. In Figs. 6(a)–(e), five different chaotic time series with their respective attractors into the phase space are represented. We note that for the first case when $a = 0.9742$ and $b = 1.42718519$ being $\lambda_1 = 0.0335602068$, the variable y has the particularity to have almost equal maxima and can also take negative values as shown in Fig. 6(a1); the distribution of points in the chaotic attractor is rather simple (Fig. 6(a2)). When $a = 0.90135135$ and $b = 0.22567167$ the LLE is $\lambda_1 = 0.0168390550$ generates the time series shown in Fig. 6(b1), where we observe that the variable y now takes only positive values, but with almost equal maxima values as in the precedent case; In what concerns the attractor, its distribution points leave some gaps, and also there is some reminiscence of comb-shaped structures in the left-lower part, as seen in Fig. 6(b2). When $a = 0.90135135$ and $b = 0.23505405$ with LLE $\lambda_1 = 0.0295812540$, the time series and the attractor in Fig. 6(c1)-(c2) are quite similar to the precedent case, but there some differences, namely, in the left lower part of the attractor that mutates its comb-shaped structure by some loops that look like petals and the other difference is that there are no distinguishable gaps in the distribution of points in the attractor. When $a = 0.90135135$

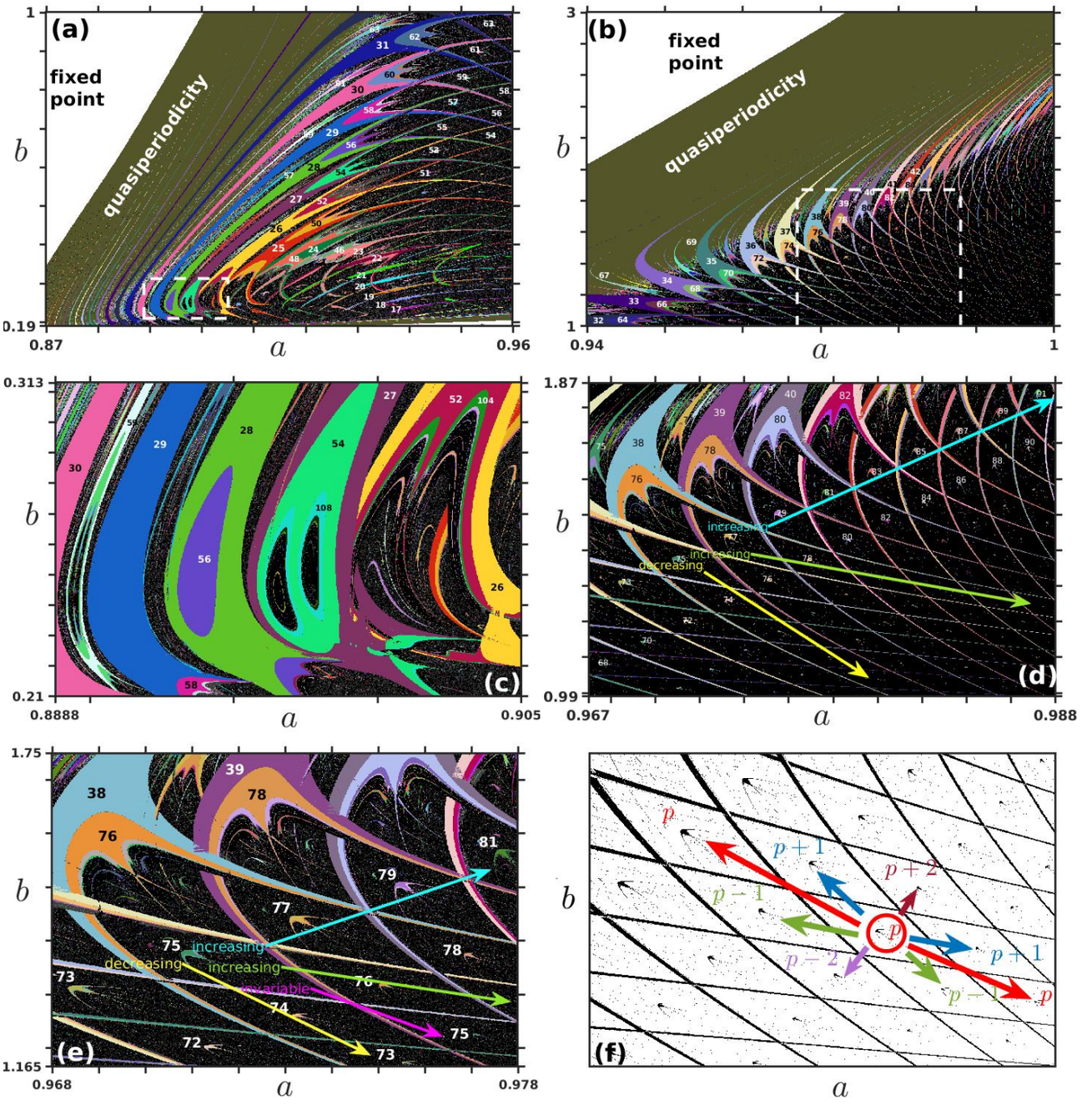

Figure 4. Parameter plane b vs a in terms of the periodicities keeping constant $c = 0.28$ and $k_0 = 0.04$ with initial conditions $x_0 = 0.1$ and $y_0 = 0.12$. (a) and (b) correspond to the same parameter planes shown in Figs. 1(b) and (c) respectively. (c) and (d) zoom of the rectangular regions shown in (a) and (b), respectively. (e) Magnification of the region in which shrimps with main periodicities of 38 and 39 and the subtended grid. As mentioned before, the colored parts of a cell on the grid represent regions in which the system behaves in a regular way as opposed to the black regions indicating chaotic behavior. (f) Sketch of how the main periodicity of the principal shrimp in each cell evolves. Conversely to the five precedent cases, in (f), the regular and chaotic behaviors are represented by black and white, respectively.

and $b = 0.22144444$ with a LLE $\lambda_1 = 0.0223690857$, the time series in Fig. 6(d1) exhibits more variability in both dynamical variables; in what concerns the attractor, its distribution of points depicts more complexity and also the emergence of some self-similar structures observable in the upper part of Fig. 6(d2). Finally, when $a = 0.90491892$ and $b = 0.21051552$ with LLE $\lambda_1 = 0.0685757018$, gives rise to a high variability on the time series of x and y as noticed in

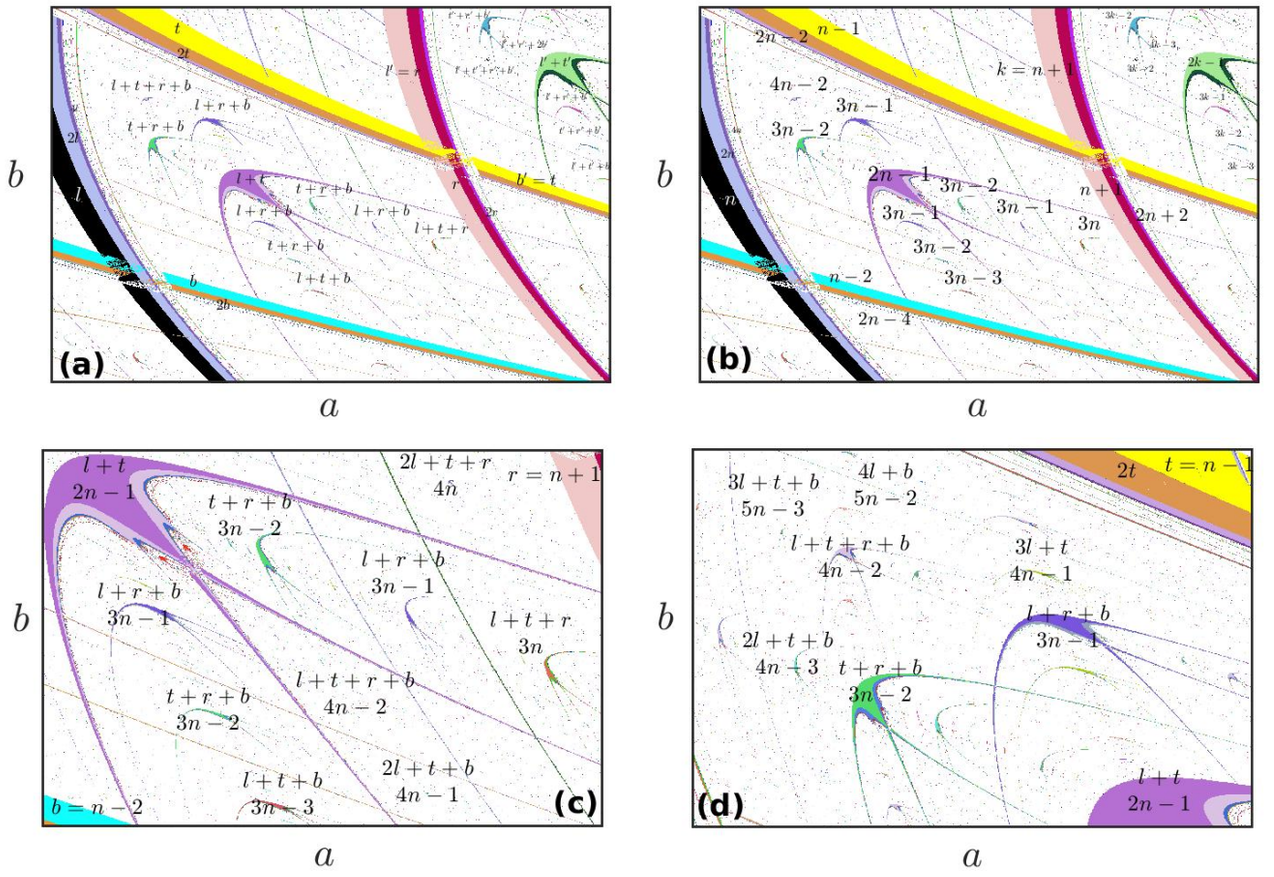

Figure 5. Representation of the periodicity's distribution in a cell of the grid shown in Fig. 3 considering the sides' periodicity (a) Being the main periodicity of the left, top, right and bottom sides, l, t, r and b respectively. (b) For the particular case in which the main periodicity of each side is: $l = n$, $t = n - 1$, $r = n + 1$ and $b = n - 2$. Magnification of (c) the primary shrimp of the cell and (d) the left-upper part of the cell; the main periodicities of selected structures in (c)–(d) are indicated using both notations: based on $(l, t, r, b$ and on n. In all cases, the white region represents chaotic behavior.

Fig. 6(e1); whereas the attractor depicts a high complexity in its distribution of points as depicted in Fig. 6(e1). Notice that for the computation of LEs, we considered a total of 10^7 and a transient of 9×10^6 and also that time series and attractors have been ordered in an apparent increasing complexity; the latter might be supported or not by the values of LLEs and the statistical values of second LE.

With the aim of characterizing the chaotic behavior for each of the five considered cases, we obtain the boxplots for the LLE (Fig. 6(f)) and the second LE (Fig. 6(g)), where we considered a Gaussian distribution with $\pm 6\sigma$; thus, the outliers might be taken as extreme events[24]. From Fig. 6(g), we note that the LLEs attain stability as expected with the coincidence of mean and median values. Considering only the value of the LLEs, we can infer that the intuitive ordering of the attractors is not the most appropriate; nevertheless, when complementing with the computation of the second LE shown in the boxplot of Fig. 6(g), we observe that according to the statistical indicators, the attractors seem to be ordered in increasing chaoticity; note the magenta horizontal line at $\lambda_2 = 0$ for facilitating the comparison. Comparing the attractors, we note that statistically (a) has a strictly negative second LE because the median (m) and the first Q_1 and third Q_3 quartiles are negatives, and consequently the interquartile range $(IQR = (Q_3 - Q_1)/2)$ lies entirely in the negative part, and also there are no outliers. For all other attractors, IQR contains negative and positive values of λ_2, and the median (m) tends to be closer to zero, especially for the attractor (e). Another observation is that the percentage of outliers is correlated with m and IQR. With the observations mentioned above and also taking into account λ_1, we propose a simple indicator of the chaoticity for each attractor in terms of the statistical measures obtained from the boxplot and λ_1 as

$$\eta = \lambda_1 + \frac{Q_3 - Q_1}{2} \times m \propto \lambda_2 \,, \tag{4}$$

indicating that it is proportional to λ_2. Although we point out the percentage of outliers (in our case, the extreme events because we work considering $\pm 6\sigma$ in the distribution), we did not include it in Eq. (4). The statistical values and the chaotic-

ity indicator for each attractor are summarized in Table I. According to the values of η, the ordering of attractors results in: (a) $\rightarrow$ (c) $\rightarrow$ (d) $\rightarrow$ (e). Moreover, in the case of the attractor (e), $\eta > 0$, it makes us think that this attractor could be statistically related to a hyperchaotic behavior.

IV. CONCLUSIONS AND PERSPECTIVES

Using parameter planes based on Lyapunov exponents and periodicities, we have unveiled several aspects of the dynamics of Chialvo's neuron model, such as the determination of clearly defined regions of regular, quasiperiodic, and chaotic behavior. We also determined the pseudofractal character of some regions of the parameter plane where the scale-free property is absent; however, self-similarity is present and described their regularities in terms of their periodicities. The description of the parameter plane in terms of the periodicities allowed us to identify the interesting structure that we called "eyes of chaos" in relationship to the structure "eye of chaos" (in singular) previously described in continuous dynamical systems. To our knowledge, it is the first time that "eyes of chaos" are reported, and with the particularity that the finding has been made in a discrete system. In the end, we described the chaoticity of some attractors considering the statistical aspects of the second Lyapunov exponent; our results open the possibility of determining the hyperchaotic features of some chaotic attractors. We expect to go in-depth into the characterization of hyperchaotic scenarios and, in this manner, complete the dynamical description of the system in terms of the parameter planes. We note that the technique of the two-parameter scan presented in the study can be applied to other neuron map models such as Rulkov map[43], Nekorkin map[32], discrete Izhikevich neuron map[22], discrete Hindmarsh-Rose neuron map[28]. This approach can reveal striking dynamical behaviors in map-based neuron models.

ACKNOWLEDGMENTS

GMRA and TK have been supported by the National Science Centre, Poland, OPUS Programs (Projects No. 2018/29/B/ST8/00457, and 2021/43/B/ST8/00641). This project has received funding from the European Union's Horizon 2020 research and innovation programme under the Marie Sklodowska-Curie grant agreement No 101034383. Computational resources have been provided by the Consortium des Équipements de Calcul Intensif (CÉCI), funded by the Fonds de la Recherche Scientifique de Belgique (F.R.S.-FNRS) under Grant No. 2.5020.11 and by the Walloon Region.

AUTHOR DECLARATIONS

Conflict of Interest

The authors have no conflicts to disclose.

Author Contributions

G. M. Ramírez-Ávila: Conceptualization (equal); Formal analysis (equal); Investigation (equal); Methodology (equal); Software (lead); Validation (equal); Visualization (equal); Writing — review & editing (equal). **S. S. Muni:** Conceptualization (equal); Formal analysis (equal); Investigation (equal); Methodology (equal); Validation (equal); Visualization (equal); Writing — review & editing (equal). **T. Kapitaniak:** Conceptualization (equal); Formal analysis (equal); Investigation (equal); Methodology (equal); Validation (equal); Visualization (equal); Writing — review & editing (equal); Resources (lead).

DATA AVAILABILITY

The data that support the findings of this study are available from the corresponding author upon reasonable request.

REFERENCES

[1]Annand, C. T., Fleming, S. M., and Holden, J. G., "Farey trees explain sequential effects in choice response time," Front. Physiol. **12** (2021).
[2]Bashkirtseva, I., Ryashko, L., Used, J., Seoane, J. M., and Sanjuán, M. A., "Noise-induced complex dynamics and synchronization in the map-based Chialvo neuron model," Commun. Nonlinear Sci. Numer. Simul. **116**, 106867 (2023).
[3]Behta, E., Goldsztein, G. H., and English, L. Q., "Phase-locking dynamics for electronic relaxation oscillators via threshold pulse-modulation: Comparing experimental and analytical Arnold tongues," Physica D **454**, 133849 (2023).
[4]Cao, H., Wang, Y., Banerjee, S., Cao, Y., and Mou, J., "A discrete Chialvo–Rulkov neuron network coupled with a novel memristor model: Design, Dynamical analysis, DSP implementation and its application," Chaos Solit. Fractals **179**, 114466 (2024).
[5]Chialvo, D. R., "Generic excitable dynamics on a two-dimensional map," Chaos Solit. Fractals **5**, 461–479 (1995).
[6]Coombes, S. and Bressloff, P. C., "Mode locking and Arnold tongues in integrate-and-fire neural oscillators," Phys. Rev. E **60**, 2086–2096 (1999).
[7]Courbage, M. and Nekorkin, V. I., "Map based models in neurodynamics," Int. J. Bifurcat. Chaos **20**, 1631–1651 (2010).
[8]Ecke, R. E., Farmer, J. D., and Umberger, D. K., "Scaling of the Arnold tongues," Nonlinearity **2**, 175–196 (1989).
[9]Elwakil, A. S. and Kennedy, M. P., "Inductorless hyperchaos generator," Microelectron. J. **30**, 739–743 (1999).
[10]Felicio, C. C. and Rech, P. C., "Arnold tongues and the devil's staircase in a discrete-time Hindmarsh–Rose neuron model," Phys. Lett. A **379**, 2845–2847 (2015).
[11]FitzHugh, R., "Mathematical models of threshold phenomena in the nerve membrane," Bull. Math. Biophys. **17**, 257–278 (1955).
[12]Freire, J. G. and Gallas, J. A., "Stern–Brocot trees in cascades of mixed-mode oscillations and canards in the extended Bonhoeffer–van der Pol and the FitzHugh–Nagumo models of excitable systems," Phys. Lett. A. **375**, 1097–1103 (2011).
[13]Gallas, J. A. C., "Dissecting shrimps: results for some one-dimensional physical models," Physica A **202**, 196–223 (1994).
[14]Gallas, J. A. C., "Periodic oscillations of the forced Brusselator," Mod. Phys. Lett. B **29**, 1530018 (2015).
[15]Gallas, J. A. C., "Non-quantum chirality in a driven Brusselator," J. Phys.-Condens. Mat. **34**, 144002 (2022).
[16]Glass, L. and Perez, R., "Fine structure of phase locking," Phys. Rev. Lett. **48**, 1772–1775 (1982).

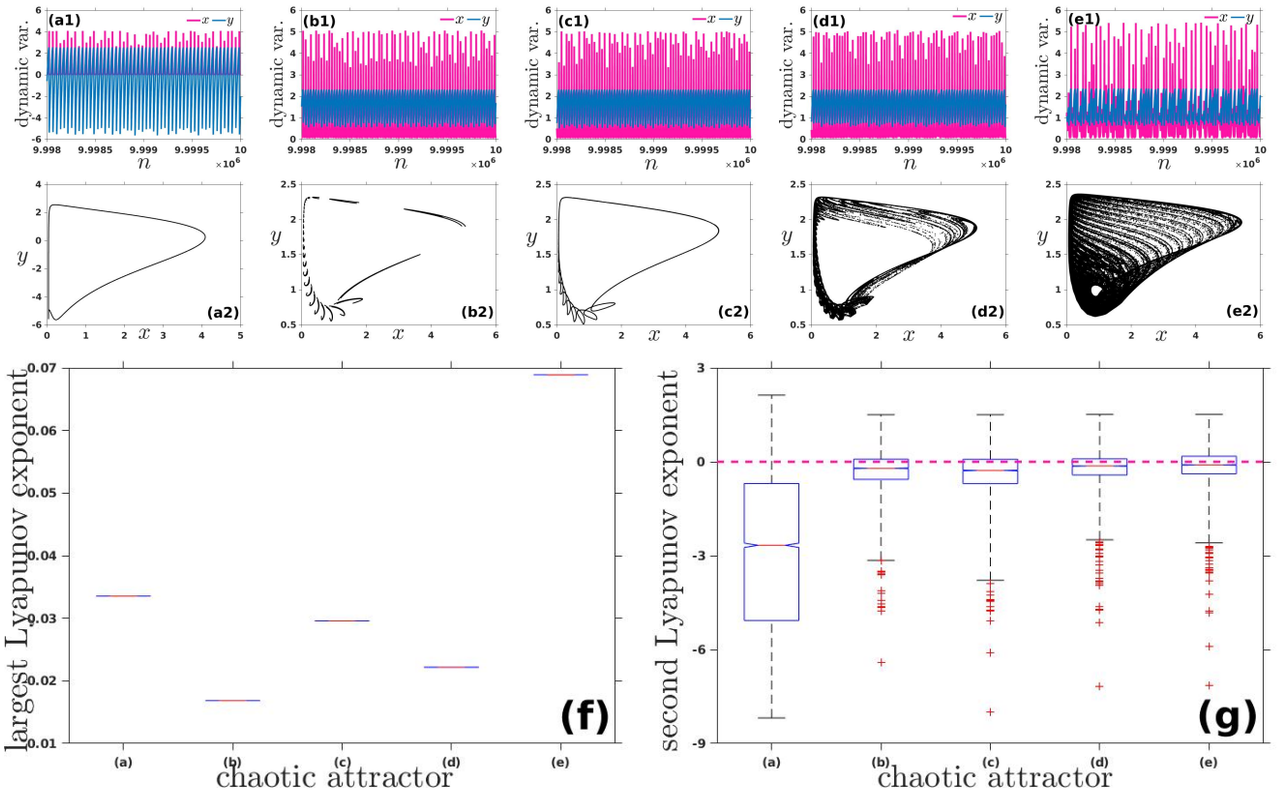

Figure 6. When keeping constant $c = 0.28$ and $k_0 = 0.04$ with initial conditions $x_0 = 0.1$ and $y_0 = 0.12$. **First row:** time series; **second row:** chaotic attractors with. (a) $a = 0.9742$ and $b = 1.42718519$ being $\lambda_1 = 0.0335602068$. (b) $a = 0.90135135$ and $b = 0.22567167$ being $\lambda_1 = 0.0168390550$. (c) $a = 0.90135135$ and $b = 0.23505405$ being $\lambda_1 = 0.0295812540$. (d) $a = 0.90135135$ and $b = 0.22144444$ being $\lambda_1 = 0.0223690857$. (e) $a = 0.90491892$ and $b = 0.21051552$ being $\lambda_1 = 0.0685757018$. **Third row:** Boxplots obtained for (f) the LLE of the five situations previously mentioned and (g) the second LE considering in both cases a Gaussian distribution with $\pm 6\sigma$.

Attractor	(a)	(b)	(c)	(d)	(e)
Minimum	-8.1845	-6.4171	-8.0052	-7.1872	-7.1452
Q_1	-5.0688	-0.56143	-0.69854	-0.42082	-0.38186
Median (m)	-2.6694	-0.21006	-0.2782	-0.13579	-0.099734
Q_3	-0.69457	0.081414	0.079198	0.090731	0.17552
Maximum	2.1308	1.5032	1.5039	1.5148	1.5142
% outliers	0	0.14	0.12	0.27	0.26
λ_1	0.0335602068	0.0168390550	0.0295812540	0.0223690857	0.0685757018
$\eta = \lambda_1 + \frac{Q_3 - Q_1}{2} \times m$	-5.8047245742	-0.05067885032	-0.0786021018	-0.012362669445	0.04078083334

Table I. Statistical values of the boxplot shown in Fig. 6(g) and a rough estimation (η) of the chaoticity of the five attractors and the possible existence of hyperchaotic behavior.

[17] Hastings, H. M., *Fractals: A User's Guide for the Natural Sciences* (Oxford University Press, 1994).
[18] Hilborn, R. C., "Quantifying Chaos," in *Chaos and Nonlinear Dynamics: An Introduction for Scientists and Engineers* (Oxford University Press, 2000).
[19] Hindmarsh, J. L., Rose, R. M., and Huxley, A. F., "A model of neuronal bursting using three coupled first order differential equations," Proc. R. Soc. Lond. B **221**, 87–102 (1984).
[20] Hodgkin, A. L. and Huxley, A. F., "A quantitative description of membrane current and its application to conduction and excitation in nerve," J. Physiol. **117(4)**, 500–544 (1952).
[21] Ibarz, B., Casado, J., and Sanjuán, M., "Map-based models in neuronal dynamics," Phys. Rep. **501**, 1–74 (2011).
[22] Izhikevich, E. M., "Simple model of spiking neurons," IEEE T. Neural Networ. **14**, 1569–1572 (2003).
[23] Jang, J. K., Ji, X., Joshi, C., Okawachi, Y., Lipson, M., and Gaeta, A. L., "Observation of Arnold tongues in coupled soliton Kerr frequency combs," Phys. Rev. Lett. **123** (2019).
[24] Kingston, S. L., Mishra, A., Balcerzak, M., Kapitaniak, T., and Dana, S. K., "Instabilities in quasiperiodic motion lead to intermittent large-intensity events in Zeeman laser," Phys. Rev. E **104**, 034215 (2021).
[25] Lin, A. L., Hagberg, A., Meron, E., and Swinney, H. L., "Resonance tongues and patterns in periodically forced reaction-diffusion systems," Phys. Rev. E **69** (2004).
[26] Main, P. B., Mosley, P. J., and Gorbach, A. V., "Revealing Arnold's Tongues in Photon-pair Generation and Quantum Frequency Conversion,"

in *OSA Advanced Photonics Congress (AP) 2020 (IPR, NP, NOMA, Networks, PVLED, PSC, SPPCom, SOF)* (Optica Publishing Group, 2020) p. JM2E.1.

[27]Mandelbrot, B., "How long is the Coast of Britain? Statistical self-similarity and fractional dimension," Science **156**, 636–638 (1967).

[28]Muni, S. S., "Mode-locked orbits, doubling of invariant curves in discrete Hindmarsh-Rose neuron model," Phys. Scr. **98**, 085205 (2023).

[29]Muni, S. S., "Ergodic and resonant torus doubling bifurcation in a three-dimensional quadratic map," Nonlinear Dyn. (2024).

[30]Muni, S. S., Fatoyinbo, H. O., and Ghosh, I., "Dynamical effects of electromagnetic flux on Chialvo neuron map: Nodal and network behaviors," Int. J. Bifurcat. Chaos **32** (2022).

[31]Munteanu, L., Brişan, C., and Chiroiu, V., "Chaos–hyperchaos transition in a class of models governed by Sommerfeld effect," Nonlinear Dyn. **78**, 1877–1889 (2014).

[32]Nekorkin, V. and Vdovin, L., "Map-based model of the neural activity," Izv. VUZ. Appl. Nonlinear Dyn. **15** (2007).

[33]Pikovsky, A. and Politi, A., *Lyapunov exponents: a tool to explore complex dynamics* (Cambridge University Press, 2016).

[34]Pilarczyk, P., Signerska-Rynkowska, J., and Graff, G., "Topological-numerical analysis of a two-dimensional discrete neuron model," Chaos **33** (2023).

[35]Rakshit, S., Ray, A., Bera, B., and Ghosh, D., "Synchronization and firing patterns of coupled Rulkov neuronal map," Nonlinear Dyn. **1**, 1–21 (2018).

[36]Ramírez-Ávila, G. M., Depickère, S., Jánosi, I. M., and Gallas, J. A. C., "Distribution of spiking and bursting in Rulkov's neuron model," Eur. Phys. J. Spec. Top. **231**, 319–328 (2022).

[37]Ramírez-Ávila, G. M. and Gallas, J. A. C., "How similar is the performance of the cubic and the piecewise-linear circuits of Chua?" Phys. Lett. A **375**, 143–148 (2010).

[38]Ramírez-Ávila, G. M., Kurths, J., and Gallas, J. A. C., "Ubiquity of ring structures in the control space of complex oscillators," Chaos **31**, 101102 (2021).

[39]Ramírez-Ávila, G. M. and Gallas, J. A. C.,, "Self-similarities in the parameter space of Chua's circuit with discrete and continuous nonlinearities (in Spanish)," Revista Boliviana de Física **18**, 1–6 (2011).

[40]Rao, X.-B., Zhao, X.-P., Gao, J.-S., and Zhang, J.-G., "Self-organizations with fast-slow time scale in a memristor-based Shinriki's circuit," Commun. Nonlinear Sci. Numer. Simul. **94**, 105569 (2021).

[41]Rosa, C., Correia, M. J., and Rech, P. C., "Arnold tongues and quasiperiodicity in a prey–predator model," Chaos Solit. Fractals **40**, 2041–2046 (2009).

[42]Rossler, O., "An equation for hyperchaos," Phys. Lett. A. **71**, 155–157 (1979).

[43]Rulkov, N. F., "Regularization of synchronized chaotic bursts," Phys. Rev. Lett. **86**, 183–186 (2001).

[44]Sekikawa, M., Kousaka, T., Tsubone, T., Inaba, N., and Okazaki, H., "Bifurcation analysis of mixed-mode oscillations and Farey trees in an extended Bonhoeffer–van der Pol oscillator," Physica D **433**, 133178 (2022).

[45]Shaw, S. W., "Arnold tongues and subharmonics in the forced oscillations of a mechanical clock," in *1985 24th IEEE Conference on Decision and Control* (1985) pp. 976–981.

[46]Smidtaite, R. and Ragulskis, M., "Finite-time divergence in chialvo hyperneuron model of nilpotent matrices," Chaos Solit. Fractals **179**, 114482 (2024).

[47]Sprott, J. C., *Chaos and time-series analysis* (Oxford University Press, New York, 2003).

[48]Stefański, K., "Modelling chaos and hyperchaos with 3-D maps," Chaos Solit. Fractals **9**, 83–93 (1998).

[49]Strelkova, G. I., Bogomolov, S. A., Rybalova, E. V., and Anishchenko, V. S., "Spatiotemporal Structures in an Ensemble of Nonlocally Coupled Nekorkin Maps," Izv. Sarat. Univ. Physics **19**, 86–94 (2019).

[50]Tappert, F. D., Goni, G. J., and Brown, M. J., "Chaos and hyperchaos in shallow water acoustics," J. Acoust. Soc. Am. **84**, S152–S152 (2005).

[51]Trujillo, F. L., Signerska-Rynkowska, J., and Bartłomiejczyk, P., "Periodic and chaotic dynamics in a map-based neuron model," Math. Methods Appl. Sci. **46**, 11906–11931 (2023).

[52]Vivekanandhan, G., Natiq, H., Merrikhi, Y., Rajagopal, K., and Jafari, S., "Dynamical analysis and synchronization of a new memristive Chialvo neuron model," Electronics **12** (2023).

[53]Wang, F. and Cao, H., "Mode locking and quasiperiodicity in a discrete-time Chialvo neuron model," Commun. Nonlinear Sci. Numer. Simul. **56**, 481–489 (2018).

[54]Wang, Y., Zhang, X., and Liang, S., "New phenomena in Rulkov map based on Poincaré cross section," Nonlinear Dyn. **111**, 19447–19458 (2023).

[55]Xu, L., Chu, Y.-D., and Yang, Q., "Novel dynamical scenario of the two-stage Colpitts oscillator," Chaos Solit. Fractals **138**, 109998 (2020).

[56]Xu, Q., Huang, L., Wang, N., Bao, H., Wu, H., and Chen, M., "Initial-offset-boosted coexisting hyperchaos in a 2D memristive Chialvo neuron map and its application in image encryption," Nonlinear Dyn. **111**, 20447–20463 (2023).